CHINESE OPTICS LETTERS

Vol. 21, No. 4 | April 2023

Effect of Ba/Sr ratio on the nonlinear optical properties of $Ba_{1-x}Sr_xTiO_3$ ($x = 0.1$–0.9) thin films

Depeng Wang (王得鹏), Ruifeng Niu (牛瑞峰), Liqi Cui (崔立棋), and Weitian Wang (王伟田)*

School of Physics and Electronic Information, Yantai University, Shandong 264005, China

*Corresponding author: wtwang@ytu.edu.cn

Received October 30, 2022 | Accepted December 16, 2022 | Posted Online March 14, 2023

Perovskite-structured barium strontium titanate ($Ba_{1-x}Sr_xTiO_3$, $x = 0.1$–0.9) films have been epitaxially fabricated by using a pulsed-laser deposition technique. The third-order nonlinear optical properties were studied through a z-scan method, allowing the resolution of the nonlinear refractive and absorptive contributions to the responses. Although all the samples show almost the same value of nonlinear absorption coefficient, the extracted nonlinear refractive index of the sample of $x = 0.3$ is apparently larger than that of other samples. Dependency of the nonlinear optical properties on the Ba/Sr ratio is discussed in terms of the crystal phase transformation and metal-oxygen bond length of the selected materials.

Keywords: nonlinear optical properties; thin films; phase transformation; pulsed-laser deposition.

DOI: 10.3788/COL202321.041601

1. Introduction

Due to their excellent dielectric properties, ferroelectric, piezoelectric, and pyroelectric effects, ABO_3 perovskite-structured materials have been studied in a wide array of cutting-edge areas of solid-state physics and materials science[1–4]. Barium titanate ($BaTiO_3$, BTO) and strontium titanate ($SrTiO_3$, STO) are the most prominent oxides because of the existing off-centered cations and lattice distortion, which can be used as bases to achieve the typical requirements by A- or B-site engineering. The solid solution of barium strontium titanate ($Ba_{1-x}Sr_xTiO_3$, BST) is a promising material, as the nonlinear behavior of dielectric and ferroelectric photorefractive properties can be tuned by adjusting the barium-to-strontium (Ba/Sr) ratio[5,6].

It has been reported that metal nanoparticles embedded in dielectric BTO or STO matrices exhibit high-order harmonic generation, which is an important factor for the development of optoelectronics, optical switchers, and nonlinear spectroscopy[7,8]. Many works focus on the third-order nonlinear optical properties of composite materials comprising gold or silver nanoparticle-embedded BTO matrices[9,10]. The enhanced optical nonlinearities in these materials were believed to originate from the giant amplification of the local electric field near the surface plasmon resonances of the nanostructured materials[11]. It should be noted that the nonlinear optical response of a composite material is related to that of its constituents. Although the optical properties of nanoparticles have been analyzed widely, the third-order nonlinear optical characteristics of BTO, STO, or BST films have been rarely reported so far.

In this Letter, a series of single-phased perovskite structure BST films were fabricated on MgO single-crystal substrates by using a pulsed-laser deposition technique. The molar concentration x was tuned from 0.1 to 0.9 to investigate the effect of a Ba/Sr ratio on the nonlinear optical properties of BST films that were studied using a single-beam z-scan method. The results show that the nonlinear absorption coefficient has a weak dependence on the Ba/Sr ratio, while the different concentration x has a considerable influence on the nonlinear refractive index.

2. Experimental Details

The pulsed-laser deposition method employing a Lambda Physic KeF excimer laser ($\lambda = 248$ nm) with a pulse width of 20 ns and a pulse energy of approximately 0.7 J per pulse was used to fabricate BST thin films on polished MgO (100) single-crystal substrates in a vacuum chamber. It has been reported that MgO crystals can be used as substrates to grow high-quality epitaxial BTO or STO films because of the lattice matching between the films and the substrate[12,13]. The BST targets, mounted on a rotating holder, were synthesized through standard solid-state reaction by using specific molar ratio and amounts of $BaCO_3$, $SrCO_3$, and TiO_2 powders with analytic reagent grade. The substrates were maintained at 650°C by a resistive heater, and the distance between the target and the substrate holder was set at 35 mm. The base pressure of the vacuum chamber was evacuated to be 1.0×10^{-4} Pa, after which the deposition was carried out under an oxygen pressure of 30 Pa.

The growth rate was monitored, and the thickness of the fabricated films was measured to be about 180 nm by using a surface profiler (Alpha-step 500, TENCOR). Five $Ba_{1-x}Sr_xTiO_3$ samples with different Ba/Sr ratios were prepared in our experiment. The values of x were set as 0.1, 0.3, 0.5, 0.7, and 0.9, and corresponding samples were named as BST01, BST03, BST05, BST07, and BST09, respectively.

The chemical state and Ba/Sr concentration in BST thin films were verified by using VGESCALab-5 X-ray photoelectron spectroscopy (XPS) with a source of Mg Kα exciting radiation ($h\nu = 1253.6$ eV). The crystallization of the prepared samples was investigated by X-ray diffraction (XRD, Bruker D8-A25 diffractometer) using Cu Kα radiation ($\lambda = 1.54$ Å, 1 Å = 0.1 nm) in the angular range of $20° \le 2\theta \le 80°$ with a step size of 0.02° and a scan step time of 0.5 s. The visible and near-infrared transparency and linear optical properties were determined by using the optical transmission spectra measured in the wavelength range of 300–800 nm.

The third-order nonlinear optical responses of the samples were studied using a single-beam z-scan technique[14]. This measurement method allows the resolution of the nonlinear refraction n_2 and nonlinear absorption β contributions to the optical nonlinearity. The experimental setup of z-scan measurement has been reported in our previous work[15]. A Nd:YAG mode-locked laser operating at 532 nm with 30 ps pulse was employed as a beam source, which was focused by using a converging lens with 120-mm focal length, leading to a beam waist of $\omega_0 = 30$ μm and a pulsed energy of $I_0 = 5.0$ μJ at the focal plane. When a sample is scanned across the focal plane, n_2 and β can be revealed by using the transmittance data through measurements with a circular aperture (closed aperture, CA) and without an aperture (open aperture, OA), respectively. The transmitted beam energy and the reference beam energy were measured by using an energy ratiometer (Rm6600, Laser Probe Corp).

3. Results and Discussion

In order to confirm the chemical state and concentration of the component elements in the BST films, XPS data were collected for the prepared samples. Typical spectra for BST03 are presented in Fig. 1. The peak positions imply the presence of Ba [Fig. 1(a)], Sr [Fig. 1(b)], Ti [Fig. 1(c)], and O [Fig. 1(d)]. The core level binding energies of Ba 3d with $3d_{5/2}$ and $3d_{3/2}$ located at 780.3 eV and 795.6 eV, respectively, indicate the existing Ba^{2+} species. The Sr 3d spectrum can be fitted with two peaks centered at 133.6 and 135.4 eV, respectively, both of which can be attributed to the Sr^{2+} oxidation state. The XPS data in Fig. 1(c) indicate the binding energies of Ti 2p are 458.7 and 464.3 eV for $2p_{3/2}$ and $2p_{1/2}$, respectively, with a spin-orbit splitting of 5.6 eV, which are characteristics of Ti^{4+}. The O 1s spectrum can be resolved into three peaks centered at 529.8, 530.7, and 531.8 eV, respectively. The peak located at 529.8 eV can be attributed to the lattice oxygen of the film. The other two peaks are possibly due to the C-O or H-O adsorptions on the film surface. The atomic ratio of Ba/Sr/Ti/O for the sample, which could be derived from the XPS data by using the corresponding peak area and atomic sensitivity factor (ASF), was calculated to be approximately 7:3:10:30. Based on the XPS results, an overall composition of BST03 can be formulated as $Ba_{0.7}Sr_{0.3}TiO_3$, which is consistent with the predetermined pattern.

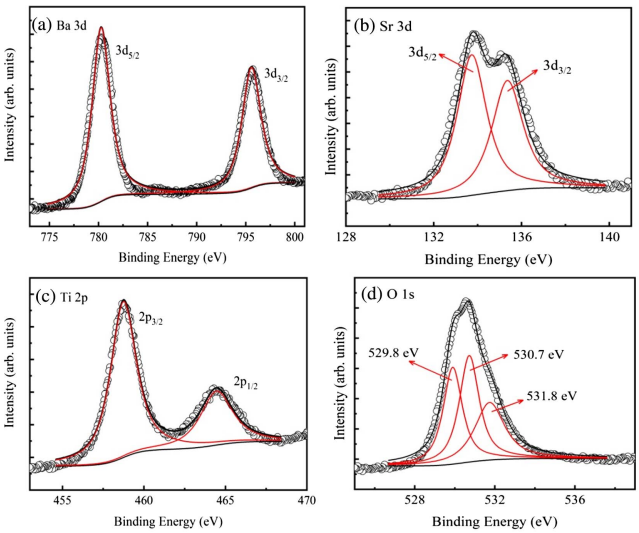

Fig. 1. Core level XPS spectra for BST03. (a) Ba 3d, (b) Sr 3d, (c) Ti 2p, and (d) O 1s. The solid lines are the fitting results using the XPS peak processing method.

Figure 2(a) shows the XRD $\theta - 2\theta$ spectra of the BST samples deposited on MgO (100) substrates. It is clear that only (00l)

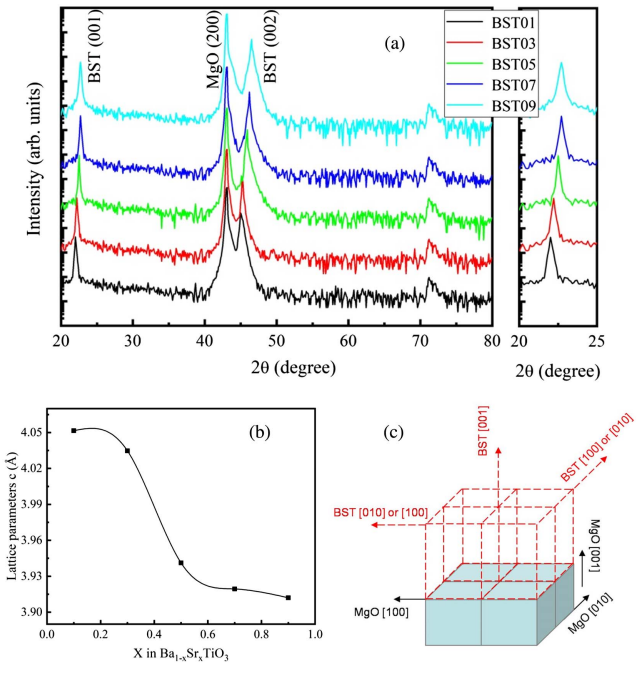

Fig. 2. (a) XRD patterns of the prepared $Ba_{1-x}Sr_xTiO_3$ films with x ranging from 0.1 to 0.9; (b) variation between the lattice parameter c and the composition x; (c) schematic display of epitaxial relationship between the film and the substrate.

peaks from perovskite-structured BST films appear in the 2θ range of 20°–80°, and no diffraction peaks from other phases can be detected, indicating the good crystallinity and fully epitaxial growth with a preferred *c*-orientation of the prepared films on MgO (100) substrates. As can be seen from Fig. 2(a), different Ba/Sr ratios have an effect on the location of diffraction peaks. The location of (001) peak shifts slightly to the high-angle direction with the increase of x, which implies a decrease of the out-of-plane lattice parameters. The calculated value of c decreases from 4.052 Å for BST01 to 3.912 Å for BST09. The variation between the composition x and the lattice parameter c is shown in Fig. 2(b). With increasing Sr concentration ($x \geq 0.5$), the c value is smaller than 3.983 Å and is close to the a-axis lattice constant. As is known, the crystal structure of $BaTiO_3$ at room temperature is tetragonal with $a = 3.994$ Å and $c = 4.038$ Å, while that of $SrTiO_3$ is cubic with $a = 3.905$ Å. The results suggest that the phases of the fabricated BST films transform from tetragonal structure for BST01 and BST03 to cubic structure for BST05, BST07, and BST09.

Although there is a certain lattice mismatch between the MgO substrate and BST films, the thermal expansion of MgO is similar to that of BST films[16]. This puts the BST films under some tensile stress for the in-plane directions, and it favors a preferred *c*-orientation for the BST films. The in-plane epitaxial relationship between BST films and MgO was supposed as BST[100] // MgO[10] and BST[10] // MgO[100], or BST[100] // MgO[100], and BST [10]//MgO [10], as schematically illustrated in Fig. 2(c).

It is widely known that linear optical properties play an important role in optical device applications. The optical transmission spectra in the wavelength range of 300–800 nm were recorded, as shown in Fig. 3. All the films display good transparency in the visible and near-infrared ranges. The oscillations in the spectra indicate the smoothness and uniformity of the films, which are caused by the optical interference. By tracing the high and low points (maxima and minima) of the oscillations, two fitting envelopes can be obtained for each sample. Typical results for BST03 are shown in the inset of Fig. 3. By denoting the values of upper and lower black lines as T_M and T_m, respectively, a numerical method can be used to determine the linear refractive n_0, which is given by a complex formula[17],

$$n_0^2 = 2n_s\frac{T_M - T_m}{T_M T_m} + \frac{n_s^2+1}{2} + \left[\left(2n_s\frac{T_M - T_m}{T_M T_m} + \frac{n_s^2+1}{2}\right)^2 - n_s^2\right]^{1/2}, \quad (1)$$

where n_s is the refractive index of the substrate.

The calculated values of n_0 for the prepared samples are shown in Fig. 4. The variation of n_0 with the incident wavelength implies the normal dispersion in the scope of measuring optical wave. At a selected wavelength $\lambda = 532$ nm, as shown in the inset of Fig. 4, BST03 ($x = 0.3$) has the largest value of n_0. With the continued increase of x ($x > 0.3$), the value of n_0 decreases monotonously.

Generally, the linear refractive index is related to the dielectric properties of transparent oxide films. The dielectric permittivity of tetragonal structured BST films is larger than that of cubic structured ones[5]. With the increase concentration of Sr, the prepared sample exhibited a tendency to transform from tetragonal phase to cubic phase, which can be seen from the XRD analysis. The phase transformation accounts for the observed results in the inset of Fig. 4.

Figure 5 shows the OA and CA z-scan results for the prepared samples. The open circles denote the normalized experimental transmittance, while the solid curves are the theoretical fits. Because the MgO substrate in our experiment has a negligible nonlinear optical response at 532 nm, which has been reported previously[18,19]; the nonlinear optical properties observed here result from the BST films. From Fig. 5(a), for all the samples, the signature of nonlinear optical saturation process is clearly seen,

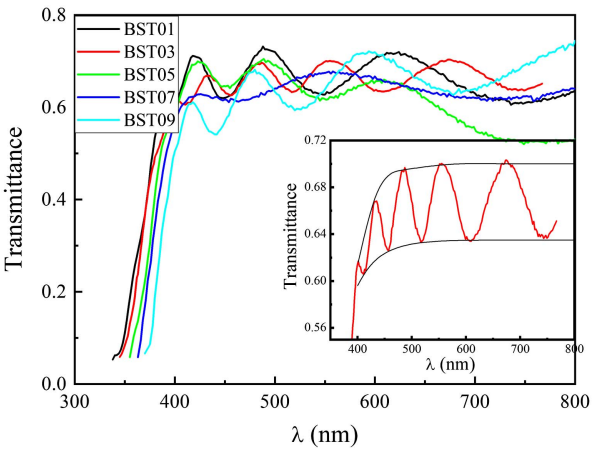

Fig. 3. Optical transmission spectra in the wavelength range of 300–800 nm for the samples; inset, simulated envelopes of the interference fringes for BST03.

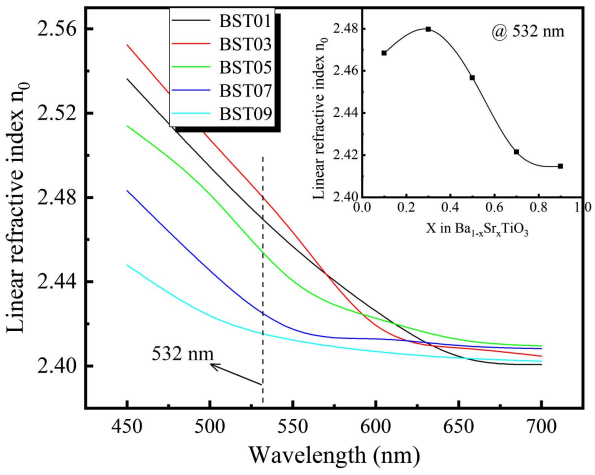

Fig. 4. Calculated linear refractive indices for the samples as a function of wavelength. The inset shows the relationship between the linear refractive index and the composition x at a typical wavelength of 532 nm.

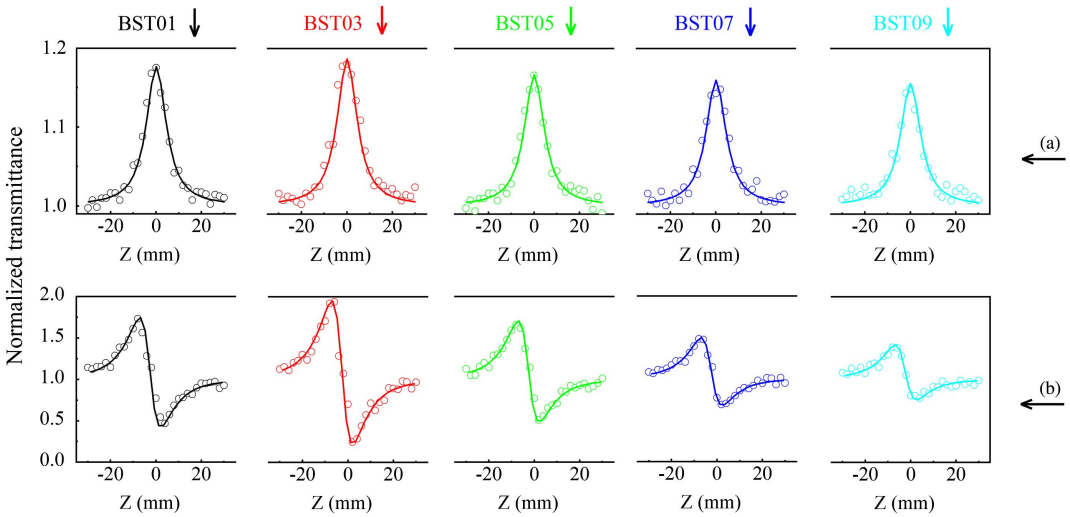

Fig. 5. (a) OA and (b) CA z-scan normalized transmittance for the samples. The solid curves are the theoretical fits to the data.

i.e., normalized transmittance peaks at the focal plane ($z = 0$). Almost the similar height of the peaks indicates approximately equal values of β for the samples. The OA data can be fitted by the following equation[20]:

$$T_{\mathrm{OA}}(z) = 1 - \frac{\beta I_0 L_{\mathrm{eff}}}{2\sqrt{2}(1 + x^2)}, \tag{2}$$

where L_{eff} is the effective thickness of the film, $x = z/z_R$, and $z_R = \pi\omega_0^2/\lambda$ is the Rayleigh length of the beam. The value of z_R of the beam was calculated to be 5.3 mm, much greater than the thickness of the fabricated samples. The calculated values of β are shown in Fig. 6. The obtained β value is in the vicinity of -0.85×10^{-7} m/W for all the samples and exhibits a weak dependence of concentration x in $Ba_{1-x}Sr_xTiO_3$.

The CA data for all the samples exhibit a peak-to-valley configuration, as shown in Fig. 5(b), indicating the existence of negative nonlinear refractive index n_2, which means there is a prefocal maximum followed by a postfocal minimum for all samples. Compared with other samples, the large peak-to-valley transmittance change observed in BST03 manifests the large value of n_2.

According to the theory of the z-scan method, the normalized CA transmittance can be described by[21]

$$T_{\mathrm{CA}}(z) = 1 - \frac{\beta I_0 L_{\mathrm{eff}}(x^2 + 3)}{(x^2 + 9)(x^2 + 1)} + \frac{2\beta I_0 L_{\mathrm{eff}} x}{\xi(x^2 + 9)(x^2 + 1)}, \tag{3}$$

where $\xi = \frac{\lambda\beta}{2\pi n_2}$.

By fitting the CA data, the n_2 value for all the prepared samples can be obtained. The variation of the calculated nonlinear refractive index n_2 with the concentration x in $Ba_{1-x}Sr_xTiO_3$ is shown in Fig. 6.

As seen from Fig. 6, the obtained n_2 decreases with the increase of x when $x > 0.3$, and the n_2 value of BST03 is about 2 times larger than that of BST09. It has been reported that the phase of $Ba_{1-x}Sr_xTiO_3$ depends on the Ba/Sr ratio[5]. When $x \leq 0.3$, this material exhibits a tetragonal ferroelectric state at room temperature. With the increase of x, the ferroelectric phase switched to the paraelectric phase. Generally, the ferroelectric materials have excellent dielectric properties. As for BST materials with different Ba/Sr ratios, $Ba_{0.7}Sr_{0.3}TiO_3$ has been reported to possess the largest dielectric constant at room temperature[5], which accounts for the large linear refractive index and nonlinear refractive index observed in BST03.

Furthermore, according to the bond-orbital theory[19], the d-orbital contributions to the nonlinear optical response increase dramatically when the metal–oxygen covalent bond length is smaller than 2 Å. For BST materials, the covalent bonding exists between the Ti and O atoms, and the Ti–O bond length varies with the phase transformation of BST. When BST crystallizes in the tetragonal phase, the unit cell extends along the c direction. The geometric configuration of the Ti–O plane of BST is shown in Fig. 7. The bond length between Ti and O (a direction) or O (b direction) is about 0.1996 Å[22]. The d-orbital

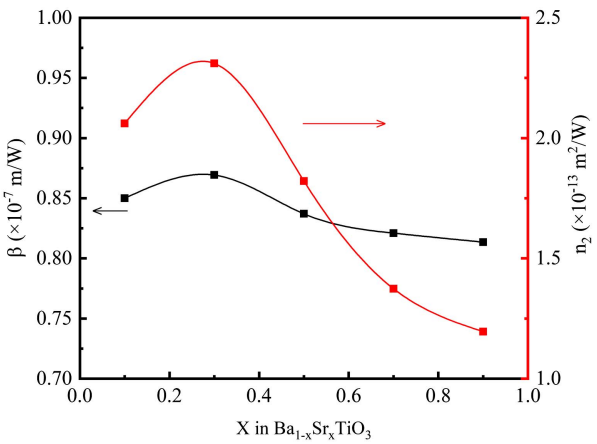

Fig. 6. The variation of n_2 and β with the concentration x in $Ba_{1-x}Sr_xTiO_3$.

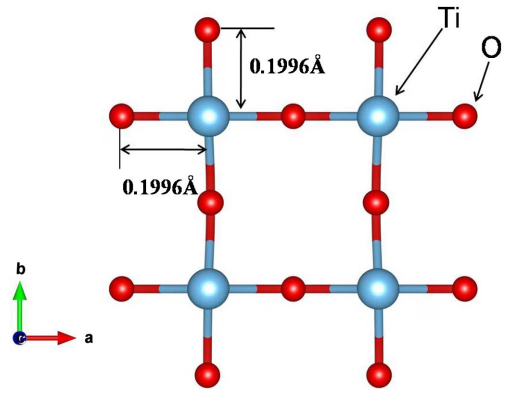

Fig. 7. Sketch of Ti-O plane of tetragonal-structured BST.

contributions play an important role for the enhancement of nonlinear optical responses in BST03 and BST01. With increasing Sr doping concentration, the crystal structure of BST transfers to a cubic phase, the Ti ions locate at the center of oxygen octahedrons, and the Ti–O bond length changes into 2.005 Å[22]. The larger bond length has no obvious effect on the nonlinear optical responses, which results in a decreased value of n_2 in BST05, BST07, and BST09.

The observed nonlinear optical saturation characteristics of the samples suggest that the fabricated BST films can be used as saturable absorbers for ultrafast pulse generation. The modulation depth and saturation intensity of the sample BST03 at 532 nm were also investigated. Figure 8 shows the variation of the normalized transmittance with the input intensity. The data were fitted using the conventional formula,

$$T(I) = 1 - \Delta M \exp\left(\frac{-I}{I_s}\right) - T_{\mathrm{ns}}, \tag{4}$$

where $T(I)$ is the normalized transmittance, ΔM is the modulation depth, T_{ns} is the nonsaturable loss, I is the input intensity,

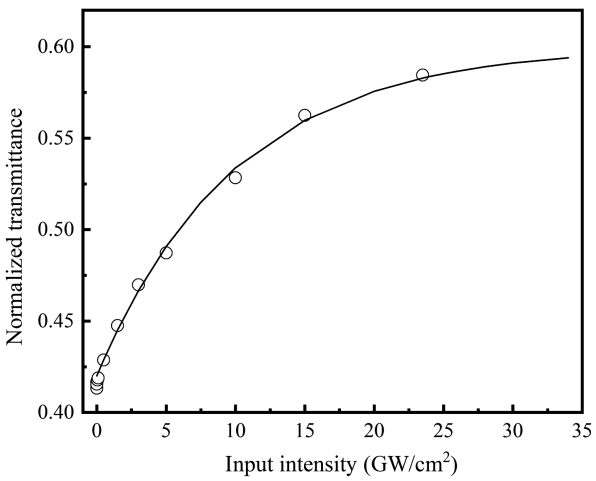

Fig. 8. Variation of the normalized transmission with the input intensity for BST03 at 532 nm. The solid line is the theoretical fitting.

and I_s is the saturation intensity. I_s and ΔM are measured to be 9.3 GW/cm^2 and 16.37%, respectively. The obtained values are comparable with those of promising saturable absorbers[23,24], suggesting that the BST films can be applied as nonlinear optical materials for optoelectronic devices.

4. Conclusions

In summary, we report the study of the linear and nonlinear optical properties of $Ba_{1-x}Sr_xTiO_3$ films as a function of the Ba/Sr ratio. The linear refractive indices of these materials were determined by using the optical transmission spectra, and the third-order nonlinear optical properties were measured through the z-scan method. The variation of Ba/Sr ratio has little effect on the nonlinear absorption but affects the nonlinear refraction significantly. The development of the nonlinear optical properties of $Ba_{1-x}Sr_xTiO_3$ films with the concentration x was explained by phase transformation and metal–oxygen bond length. These results show the capability of controlling the nonlinear optical properties of these solid solution oxides through the physical parameters of fabrication.

Acknowledgement

This work was supported by the National Natural Science Foundation of China (No. 10704065) and the Graduate Innovation Foundation of Yantai University (No. KGIFYTU2212).

References

1. X. G. Zhao, O. I. Malyi, and A. Zunger, "Intrinsic local symmetry breaking in nominally cubic paraelectric $BaTiO_3$," Phys. Rev. B **105**, 224108 (2022).
2. M. Yalcin, D. Ozmen, D. K. Takci, and F. Yakuphanoglu, "Synthesis, structural, optical and dielectric characterization of $Y_{1-x}Sr_xCuO_3$ nanoceramics," Chem. Phys. Lett. **792**, 139404 (2022).
3. A. Watras, R. Pązik, and P. J. Dereń, "Optical properties of Ce^{3+} doped ABO_3 perovskites (A=La, Gd, Y and B=Al, Ga, Sc)," J. Lumin. **133**, 35 (2013).
4. A. Paul, A. Mukherjee, I. Dasgupta, A. Paramekanti, and T. Saha-Dasgupta, "Hybridization- switching induced Mott transition in ABO_3 perovskites," Phys. Rev. Lett. **122**, 016404 (2019).
5. H. A. Gatea and I. S. Naji, "The effect of Ba/Sr ratio on the Curie temperature for erroelectric barium strontium titanate ceramics," J. Adv. Dielectr. **10**, 2050021 (2020).
6. Z. Xu, D. Yan, D. Xiao, P. Yu, and J. Zhu, "Dielectric enhancement of $BaSrTi_{1.1}O_3/BaSrTi_{1.05}O_3/BaSrTiO_3$ multilayer thin films prepared by RF magnetron sputtering," Ceram. Int. **39**, 1639 (2013).
7. R. A. Ganeev, M. Suzuki, M. Baba, M. Ichihara, and H. Kuroda, "Low- and high-order nonlinear optical properties of $BaTiO_3$ and $SrTiO_3$ nanoparticles," J. Opt. Soc. Am. B **25**, 325 (2008).
8. A. J. Piña-Díaza, D. Torres-Torresb, M. Trejo-Valdezc, C. R. Torres-SanMiguela, C. L. Martínez-Gonzáleza, and C. Torres-Torresa, "Decision making two-wave mixing with rotating TiO_2-supported Au-Pt nanoparticles," Opt. Laser Technol. **119**, 105638 (2019).
9. D. Guan, Z. Chen, K. Jin, and G. Yang, "Ultrafast nonlinear optical response of Ag:$BaTiO_3$ composite films at the near-ultraviolet wavelengths," Chin. Opt. Lett. **4**, 370 (2006).
10. W. T. Wang, Z. H. Chen, G. Yang, D. Y. Guan, G. Z. Yang, Y. L. Zhou, and H. B. Lu, "Resonant absorption quenching and enhancement of optical

nonlinearity in Au:$BaTiO_3$ composite films by adding Fe nanoclusters," Appl. Phys. Lett. **83**, 1983 (2003).
11. B. Guo, Z. Zhang, Y. Huo, S. Wang, and T. Ning, "Modulation of epsilon-near-zero wavelength and enhancement of third-order optical nonlinearity in ITO/Au multilayer films," Chin. Opt. Lett. **21**, 013602 (2023).
12. W. Zhang, B. W. Peng, L. M. Kang, F. R. Hu, H. B. Cheng, and Y. J. Wang, "Grain texture dependent charge transport behaviors and dielectric responses of $BaTiO_3$ films fabricated on MgO substrates," Mater. Res. Bull. **145**, 111553 (2021).
13. J. C. Chen, A. Ito, and T. Goto, "High-speed epitaxial growth of $SrTiO_3$ films on MgO substrates by laser chemical vapor deposition," Ceram. Int. **42**, 9981 (2016).
14. M. Sheik-Bahae, A. A. Said, T. H. Wei, D. J. Hagan, and E. W. Van Stryland, "Sensitive measurement of optical nonlinearities using a single beam," IEEE J. Quantum Electron. **26**, 760 (1990).
15. L. Cui, R. Niu, and W. Wang, "Third-order optical nonlinearity of indium-doped rutile TiO_2 thin films," Opt. Eng. **61**, 057105 (2022).
16. C. Buchal, L. Beckers, A. Eckau, J. Schubert, and W. Zander, "Epitaxial $BaTiO_3$ thin films on MgO," Mater. Sci. Eng. B **56**, 234 (1998).
17. I. Chambouleyron, J. M. Martinez, A. C. Moretti, and M. Mulato, "Retrieval of optical constants and thickness of thin films from transmission spectra," Appl. Opt. **36**, 8238 (1997).
18. W. Wang, G. Yang, Z. Chen, H. Lu, Y. Zhou, G. Yang, and X. Kong, "Nonlinear refraction and saturable absorption in Au:$BaTiO_3$ composite films," Appl. Opt. **42**, 5591 (2003).
19. M. E. Lines, "Influence of d orbitals on the nonlinear optical response of transparent transition-metal oxides," Phys. Rev. B **43**, 11978 (1991).
20. P. B. Chapple, J. Staromlynska, J. A. Hermann, and T. J. Mckay, "Single-beam Z-scan: measurement techniques and analysis," J. Nonlinear Opt. Phys. Mater. **6**, 251 (1997).
21. X. Liu, S. Guo, H. Wang, and L. Hou, "Theoretical study on the closed-aperture Z-scan curves in the materials with nonlinear refraction and strong nonlinear absorption," Opt. Commun. **197**, 431 (2001).
22. W. D. Xue, Z. Y. Chen, C. Yang, and Y. R. Li, "First principles study on tetragonal $BaTiO_3$ ferroelectric," Acta. Phys. Sin. **54**, 857 (2005).
23. X. He, H. Zhang, R. Wei, Z. Ma, J. Qiu, M. Zhang, Q. Zeng, A. Liu, and R. He, "Nonlinear saturable absorption of nanoscaled Bi_2Te_3/PMMA composite film," Physica E **81**, 71 (2016).
24. Z. Wang, H. Mu, J. Yuan, C. Zhao, Q. Bao, and H. Zhang, "Graphene-Bi_2Te_3 heterostructure as broadband saturable absorber for ultra-short pulse generation in Er-doped and Yb-doped fiber lasers," IEEE J. Sel. Top. Quantum Electron. **23**, 8800105 (2017).